

RSC Advances



This is an *Accepted Manuscript*, which has been through the Royal Society of Chemistry peer review process and has been accepted for publication.

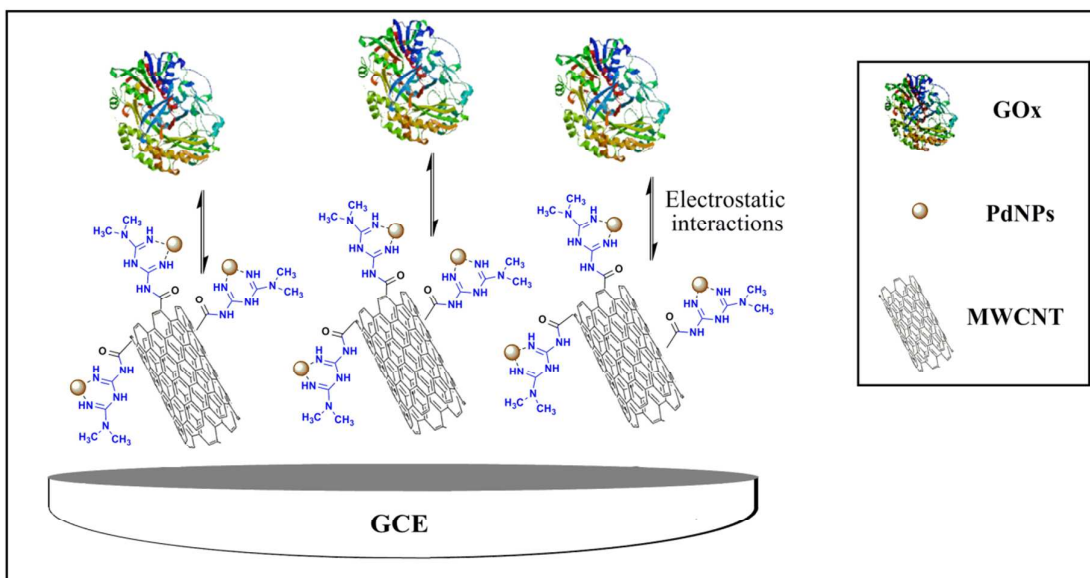
Accepted Manuscripts are published online shortly after acceptance, before technical editing, formatting and proof reading. Using this free service, authors can make their results available to the community, in citable form, before we publish the edited article. This *Accepted Manuscript* will be replaced by the edited, formatted and paginated article as soon as this is available.

You can find more information about *Accepted Manuscripts* in the [Information for Authors](#).

Please note that technical editing may introduce minor changes to the text and/or graphics, which may alter content. The journal's standard [Terms & Conditions](#) and the [Ethical guidelines](#) still apply. In no event shall the Royal Society of Chemistry be held responsible for any errors or omissions in this *Accepted Manuscript* or any consequences arising from the use of any information it contains.

Table of contents entry

Sensitive detection of glucose using a glassy carbon electrode modified with glucose oxidase and multi-walled carbon nanotubes decorated with palladium nanoparticles



Multi-walled carbon nanotubes decorated with palladium nanoparticles as a novel platform for electrocatalytic sensing applications

Mehdi Baghayeri^{a,*}, Hojat Veisi^b, Hamed Veisi^c, Behrooz Maleki^a, Hassan Karimi-Maleh^d and Hadi Beitollahi^e

^aDepartment of Chemistry, Faculty of Science, Hakim Sabzevari University, P.O. Box 397, Sabzevar, Iran

^bDepartment of Chemistry, Payame Noor University, 19395-4697 Tehran, Iran

^cDepartment of Nanomedicine, School of Advanced Medical Sciences and Technologies, Shiraz University of Medical Sciences, Shiraz, Iran

^dDepartment of Chemistry, Graduate University of Advanced Technology, Kerman, Iran

^eEnvironment Department, Institute of Science and High Technology and Environmental Sciences, Graduate University of Advanced Technology, Kerman, Iran

*Corresponding author. Tel: +98 5714003325; fax: +98 5714003170

E-mail address: m.baghayeri@hsu.ac.ir

Abstract

A simple method to decorate multi-walled carbon nanotubes (MWCNTs) with palladium nanoparticles (PdNPs) is illustrated. MWCNTs were functionalized via C–C covalent bond with metformine (Met/fMWCNT). The subsequent bonding of the imine groups with palladium offered strong adhesion of PdNPs on functionalized MWCNT surface (Pd@Met/fMWCNT). The structure and morphology of the resulting MWCNT-based nanocomposite were characterized by transmission electron microscopy, X-ray diffraction and FT-IR. Pd@Met/fMWCNT nanocomposite was used to immobilize glucose oxidase (GOx) on glassy carbon electrode. Detailed electrochemical analysis was performed and it was found that Pd@Met/fMWCNT nanocomposite significantly improved the direct electron transfer between GOx and glassy carbon electrode, leading to the fabrication of a biosensor with a very sensitive detection of glucose. The surface coverage of GOx and the electron transfer rate constant (k_s) were calculated to be 4.17×10^{-10} mol cm⁻² and 3.24 s⁻¹, respectively. The apparent Michaelis-Menten constant of the immobilized GOx was 0.48 mM, implying a fabulous catalytic activity and a remarkable affinity of the immobilized GOx for glucose. The linear detection range of glucose was 4.0-1500 μM, with a detection limit of 1.4 ± 0.04 μM.

Keywords: Glucose biosensor; Palladium nanoparticles; Direct electron transfer; Glucose oxidase

1. Introduction

In recent decades, great efforts have been assigned to improve molecular sensing or recognizing systems for the chemically and biologically important molecules.¹⁻⁶ Electrochemical biosensors, capable of a direct transduction of the biomolecular recognition event into an electronic signal, enabling lower detection limits are gaining interest for sensitive and specific detection of a target analyte.⁷ However, to realize a biosensor with improved parameters such as selectivity and stability, which depend on the biosensing molecule attachment and its compatibility with the solid surface, requires extensive investigations.^{8,9} Biosensor development using carbon nanotubes (CNTs) and electrochemical techniques has recently been employed,¹⁰ where CNT existence allows the binding of biomolecules in the closest vicinity of the electrode surface, and the electrochemical detection technique results in enhanced sensitivity, fast response, low cost, and portability.^{11,12} Moreover, the higher conductivity and better charge transfer channels of CNTs make them a most promising material for biomolecular immobilization applications.^{13,14} In the recent years, MWCNTs have emerged to be one of the most intensively investigated nanostructured materials.¹⁵ It was also observed that the chemical functionalization of MWCNTs enhances the specific surface area and thereby improves the electrical conductivity, mechanical properties and compatible for the immobilization of biomolecules.^{16,17} The subtle properties of functionalized MWCNTs render them very attractive candidates for use as nanotemplates for the dispersion and stabilization of nanomaterials. Among various nanomaterials, metal nanoparticles with well-defined surfaces have attracted significant attention in many research areas, owing to their extraordinary catalytic, magnetic and optical properties.^{18,19} Generally, the electrocatalytic activity of metal nanoparticles evidently depends on the nature, generation, size and kind of the functional groups available on the support.^{18,20-22} Several methods have been developed to attach metal

nanoparticles to CNTs. Yu et al. showed that deposition of well-dispersed Pt as small metal clusters (10-20 nm) onto functionalized carbon nanotubes can be achieved when the nanotubes are previously oxidized by HNO₃ or H₂SO₄-HNO₃ mixture;²³ Sun et al. reported an approach to highly dispersed Pd nanoparticles on covalent functional MWCNT surfaces;²² Zanella et al. reported deposition of gold nanoparticles onto thiol-functionalized MWCNTs.²⁴

Determination of glucose has an importance in biological fluids such as blood and urine for the diagnosis and the treatment of diabetic patients.²⁵ As is well known, diabetes is a worldwide public health problem.²⁶ Reagentless glucose biosensors based on the direct electrochemistry of glucose oxidase (GOx) play a leading role in the monitoring of serum or urine glucose levels.²⁷ However, the two bound redox-active flavin adenine dinucleotide cofactors of GOx are deeply buried within the insulated prosthetic shells, rendering them inaccessible for direct electron transfer (DET) with bare electrodes.²⁷ Intensive efforts have been devoted to the development of retention of the biological activity and promote DET behaviors of GOx via selected matrix.²⁷⁻³¹ Such matrixes as a biosensor platform not only must present an abundant domain for biomolecular binding but also fast electron transfer of enzyme and further amplify the electrochemical signal.

In the present work, synthesis of a novel nanocomposite based on heterogeneous palladium nanoparticles (PdNPs) supported on MWCNTs surface chemically functionalized with metformine (Pd@Met/fMWCNT) was reported. Subsequently, the Pd@Met/fMWCNT nanocomposite was casted on the glassy carbon electrode surface (Pd@Met/fMWCNT/GCE) and successfully applied in studying the immobilization and DET of GOx for the first time (GOx-Pd@Met/fMWCNT/GCE). Experimental results demonstrate that the Pd@Met/fMWCNT nanocomposite can be a good candidate for enzyme immobilization and preparation of biosensors based on the direct electrochemistry of enzymes without any electron transfer mediator. Modifying a Pd@Met/fMWCNT nanocomposite on a GCE

surface has several advantages: (1) The metformine is modified on a MWCNT surface via a C–C covalent bond which is strong and suitable as substrate for nanoparticles deposition. (2) Covalent bonding of two-dimensional metformine monolayer on the MWCNT surface provides a uniform functional surface, which can directly increase the effective interaction and chemical fixation of GOx. (3) PdNPs supported on Pd@Met/fMWCNT nanocomposite can gratify the lack of good electrical communication between the biomaterial components and the electronic elements as a major obstacle in biosensor fabrication as well as their catalytic role in fabrication of biosensor. Totally, combine with the electrical/mechanical properties of fMWCNT, the catalytic abilities of both Met and PdNPs, the resultant nanocomposite is more biocompatible and it offers a favorable microenvironment for facilitating DET between GOx and electrode. Furthermore, the adsorbed GOx retains its native structure and bioactivity activities to glucose, indicating a new reagentless amperometric glucose biosensor can be constructed based on this new nanocomposite.

2. Experimental

2.1 Materials

Glucose oxidase (GOx, from *Aspergillusniger*, EC1.1.3.4.150,000 unit/g) and glucose (Sigma, 99%) were purchased from USA and used without further purification. MWCNTs (>95%, O.D.: 10-15 nm, I.D.: 2-6 nm, length: 0.1-10 μm) were purchased from Sigma–Aldrich. SOCl_2 , HCl, H_2SO_4 , HNO_3 , H_2O_2 (30 wt.%, aq), deionized water, NaH (80%), anhydrous dimethylformamide (DMF), CaH_2 , and metformin hydrochloride were obtained from Sigma Aldrich and Merck. Phosphate buffer solutions (PBS) were prepared by mixing the stock solutions of 0.1 M NaH_2PO_4 and 0.1 M Na_2HPO_4 , and then adjusting the pH with H_3PO_4 or NaOH. The glucose stock solution was prepared by 0.1 M pH 7.0 PBS. All other chemicals were of analytical grade and were used as received without any purification

process. All the supplementary chemicals were of analytical grades and solutions were prepared with 18.2 M Ω deionized water. The supporting electrolytes were used in all the experiments with 0.1 M PBS.

2.2 Apparatus and instrumentations

Autolab Electrochemistry Instruments (Autolab, Eco Chemie, Netherlands) was used for amperometry measurements and electrochemical impedance spectroscopy (EIS). Cyclic voltammetry measurements were carried out on a Metrohm (797 VA Computrace, Switzerland) controlled by personal computer. A saturated calomel electrode (SCE) as reference electrode and a platinum wire as auxiliary electrode were used. A glassy carbon electrode (GCE), Metrohm, Switzerland, with a geometrical area of 0.0314 cm², bare or modified, was used as working electrode. EIS was performed in 1.0 mM K₃Fe(CN)₆/K₄Fe(CN)₆ (1/1) mixture with 0.1 M KCl as supporting electrolyte, using an alternating current voltage of 5 mV, within the frequency range of 0.1–10⁵ Hz. FT-IR spectra were recorded on a Bruker Tensor 27 spectrometer (Bruker, karlsruhe, Germany). All experiments were performed at room temperature (25 \pm 2 °C). X-ray diffraction (XRD, Rigaku Corporation, Tokyo, Japan) patterns were obtained at room temperature on a Rigaku kuD/Max-2550 powder diffractometer with a scanning rate of 5° min⁻¹, and recorded in the 2 θ range of 10-70 °C. Transmission electron microscopy, TEM, (Zeiss, EM10C, 80 kV) was used to obtain information on the particle size and morphology of nanocomposite. A digital pH-meter (780 pH meter, Metrohm) with precision of \pm 0.001 was used to read the pH value of the buffer solutions. Electrolyte solutions were deoxygenated by purging pure nitrogen (99.99%) for 10 min prior to electrochemical experiments. All measurements were carried out under a nitrogen atmosphere.

2.3 Preparation of free metformin

1.65 g of metformin hydrochloride (10 mmol) and 0.40 g of NaOH (10 mmol) were added to 100 ml of ethanol and the resulting suspension was stirred for 5 h. Then, the suspension was filtered and ethanol was removed with rotary evaporation leading to free metformin in 99% yield. The obtained free metformin was freshly used in the next experiments.

2.4 Chemical functionalization of MWCNTs

MWCNTs were chemically functionalized according to previously reported chemical routes for covalent functionalization.^{16,32} Briefly, pristine MWCNTs (p-MWCNTs) were refluxed under stirring in the mixture of concentrated H₂SO₄/HNO₃ (3:1) at 70 °C for 30 h for the generation of oxygen-containing functional groups, which was followed by centrifugation and repeated washings with deionized water. The carboxylated MWCNTs (MWCNTs-COOH) was then dried at 50 °C in vacuum overnight. The carboxylated MWCNTs were suspended in a mixture of 50 mL thionyl chloride and 2 mL DMF and were further refluxed. The acyl-chlorinated MWCNT derivatives were centrifuged, washed with anhydrous THF, and dried under vacuum at 50 °C for 12 h. The final product was then subjected to functionalization with metformine. Free metformine (metformine-to-MWCNTs weight ratio was 10:1) were mixed with 1 mL solution of DMF and NaH (80%) and then stirred for 1 hour. The obtained acyl chloride MWCNTs in 20 mL DMF were then added to the suspension. The reaction mixture was kept at 120 °C for 3 days. The solid was then separated by filtration and washed with CH₂Cl₂ and deionized water for several times and dried in vacuum at room temperature and collected as black powder.

2.5 Preparation of Pd@Met/fMWCNT nanocomposite

Covalently functionalized MWCNT with metformine (Met/fMWCNT) was further functionalized with PdNPs thus occurring a novel nanocomposite material: Pd@Met/fMWCNT. Scheme 1A shows the schematic representation for the preparation of Pd@Met/fMWCNT nanocomposite. In brief, an aqueous solution of PdCl₂ (10 mL, 0.6 mmol) was added to a dispersion of Met/fMWCNT (1 g) in acetonitrile (30 mL) and sonicated for 10 min. The mixture was stirred for 24 h in room temperature to complete attainment of coordination (Pd²⁺@Met/fMWCNT). The obtained Pd²⁺@Met/fMWCNT material was subjected to centrifugation washed with acetonitrile and deionized water and dried in vacuum at 40 °C for 12 h. For the preparation of Pd@Met/fMWCNT nanocomposite, in a typical experiment 100 μL of hydrazine hydrate (80%) was added to 30 mg colloidal solution of Pd²⁺@Met/fMWCNT in 60 mL of water followed by adjustment of pH to 10 via addition of ammonium hydroxide (25%) with stirring at 95 °C for 2 h. The final Pd@Met/fMWCNT nanocomposite was washed with water and dried in vacuum at 50 °C.

Scheme 1

2.6 Preparation of Pd@Met/fMWCNT nanocomposite-modified electrode

The glassy carbon electrode was prepared by a simple casting method. Prior to use, the GCE was polished with 1.0 and 0.3 μm alumina powder respectively to obtain mirror like surface and rinsed with doubly distilled water, followed by sonication in ethanol solution and doubly distilled water successively. Then 15 cycles scans were carried out in the potential range of -2.0 to +2.0 V vs. reference electrode in a solution of 1 M H₂SO₄. Finally, the electrode was thoroughly washed with deionized water and dried for 3 min at 40 °C in an oven. The nanocomposite (0.5 mg) was kept on ultrasonic dispersing for 3 min in methanol (0.5 mL, 0.5%) solution. The obtained suspension (6 μL) was then cast onto the GCE and dried in air at room temperature. The modified electrode can be expressed as

Pd@Met/fMWCNT/GCE. Then, 6 μL of 2.5 mg/mL GOx in 0.1 M PBS of pH 5 was dropped on the Pd@Met/fMWCNT/GCE, and allowed to dry in refrigerator at 4 $^{\circ}\text{C}$ for 5 h. Finally, the GOx-immobilized electrode was rinsed throughout with 0.1 M pH 7.0 PBS to wash away the loosely adsorbed GOx molecules (Scheme 1B). The obtained electrode was labeled as GOx-Pd@Met/fMWCNT/GCE. To compare with GOx-Pd@Met/fMWCNT/GCE, GOx-GCE, GOx-Met/fMWCNT/GCE and GOx-fMWCNT/GCE were also fabricated according to the same casting method.

3. Results and Discussion

3.1 Structural and Morphological Studies

The morphological characteristics of the Met/fMWCNT and Pd@Met/fMWCNT nanocomposite are analyzed by TEM. Fig. 1A represents the TEM image of Met/fMWCNT, which shows that the average diameter of the Met/fMWCNT was 15-20 nm. Fig. 1B is a typical TEM image of Pd@Met/fMWCNT nanocomposite showing that the MWCNTs covered with a continuous PdNPs adlayer, extend the overall length of MWCNTs. It can be seen that although PdNPs are distributed on MWCNTs, they do not aggregate with each other, because the imine groups of metformine effectively isolate adjacent PdNPs. The average PdNPs size is 5-10 nm.

"Figure 1"

Furthermore, the XRD pattern of Pd@Met/fMWCNT nanocomposite is shown in Fig. 2. As seen from Fig. 2, the wide diffraction peak at $2\theta = 25^{\circ}$ can be indexed to disorderedly stacked hexagonal graphite structure. It is obviously seen that there are several strong reflection peaks at 2θ values of 40° , 47° , 68° and 83° , these peaks can be well-assigned to

(111), (200), (220) and (311) crystal planes of Pd⁰. Thus the XRD results indicate efficient immobilization of *fcc* structured PdNPs on Met/fMWCNT nanocomposite.

"Figure 2"

FT-IR spectra were recorded to characterize the structure of Pd@Met/fMWCNT nanocomposite and illuminate the existing state of the adsorbed GOx. Fig. 3 shows the FT-IR spectra of (a) p-MWCNTs, (b) MWCNT-COOH, (c) MWCNT-COCl, (d) Met/fMWCNT, and (e) Pd@Met/fMWCNT samples. Fig. 3, curve a, is the FT-IR spectra of p-MWCNTs. As it is seen in the curve b, the band at 1728 cm⁻¹ is corresponding to carbonyl stretch of the carboxylic acid group. The converting of the carboxylic acid groups (MWCNT-COOH) into the acyl chloride intermediate (MWCNT-COCl) by treatment with thionyl chloride was confirmed by the appearance of peak near 1778 cm⁻¹ stretching in curve c. Curve d shows the spectrum of Met/fMWCNT and the absorption band at 1658 cm⁻¹ was attributed to the carbonyl stretching of the amide groups (-CONH-). Also, the band in the spectral region of 1671 cm⁻¹ can be assigned to the imine (C=NH) bond of the attached metformine. These results indicated that the metformine was bonded to the surface of MWCNTs through amidation reaction. The signals appeared at 1671 and 1658 cm⁻¹ in curve d for the metal-ligand co-ordination presumably leads to a shift of these two peaks to lower frequencies (1671 to 1656 cm⁻¹). This shift can be observed comparing curve e. These peaks at curves d and e displayed the successful attachment of metformine organic ligands and subsequent coordination of PdNPs within the hybride material.

"Figure 3"

The interaction between Pd@Met/fMWCNT nanocomposite and GOx are evaluated in Fig. 4. A comparison with pure Pd@Met/fMWCNT nanocomposite (curve a) and native GOx (curve b) confirms the incorporation of GOx into Pd@Met/fMWCNT nanocomposite (curve c). For native GOx (curve b), the intense absorption at 3409 cm^{-1} is assigned to the N–H stretching, and the characteristic peaks were observed at 1624 and 1537 cm^{-1} , which are attributed to amide I (the C=O stretching vibrations of the peptide bond groups) and II (the N–H in-plane bending and C–N stretching modes of the polypeptide chains) bands of native GOx.³³ The spectrum of GOx–Pd@Met/fMWCNT (curve c) also shows two characteristic adsorption bands at 1630 and 1542 cm^{-1} , suggesting that GOx has been successfully immobilized on the Pd@Met/fMWCNT nanocomposite. The slight shift of the adsorption bands corresponding to amide I and II may come from intermolecular interaction between enzyme and Pd@Met/fMWCNT nanocomposite, which can effectively prevent the leaching of GOx from the Pd@Met/fMWCNT nanocomposite. These results prove that the fabricated Pd@Met/fMWCNT nanocomposite provide a favorable microenvironment for the enzyme to maintain its good bioactivity.

"Figure 4"

3.2 Electrochemical Impedance Spectroscopy

EIS is a very useful technique for the determination of electrochemical frequency behavior of surface-modified electrodes. It gives information about the charge transport behavior of the electrode material at the electrode/electrolyte interface. A Nyquist plot is the most extensively used plot for the EIS analysis. It is the plot of real component (Z') of the impedance with the imaginary component (Z''). Fig. 5A shows the Nyquist plots of the bare GCE (curve a), Pd@Met/fMWCNT/GCE (curve b), and GOx–Pd@Met/fMWCNT/GCE (curve c), respectively, recorded at the open circuit potential in a 3.0 mM 1:1

$K_3[Fe(CN)_6]/K_4[Fe(CN)_6]$ solution. The area at higher frequency represents the electrolyte properties, and the region in the middle frequency is related to the electrode/electrolyte interface processes. The intercepts of the curves with the real axis is the solution resistance (R_s), and the depressed semicircle at the higher frequency region represents the charge transfer resistance (R_{ct}) of the electrode materials. From the Nyquist plot the charge-transfer resistance of 0.78 and 0.50 k Ω have been determined for bare GCE and Pd@Met/fMWCNT/GCE, respectively. The lowest R_{ct} value of the Pd@Met/fMWCNT/GCE indicates that the Pd@Met/fMWCNT nanocomposite can decrease the charge-transfer resistance of the GCE. When GOx immobilize on the Pd@Met/fMWCNT nanocomposite, the R_{ct} increased to 1.4 k Ω . These results indicate that GOx was steadily immobilized on the Pd@Met/fMWCNT nanocomposite, causing the inhibition of the electron transfer of redox couple.³³

"Figure 5"

3.3 Direct electrochemistry of GOx

Fig. 5B shows cyclic voltammograms (CVs) of the GOx-GCE (a), GOx-fMWCNT/GCE (b), GOx-Met/fMWCNT/GCE (c) and GOx-Pd@Met/fMWCNT/GCE (d) in N_2 -saturated 0.1 M pH 7.0 PBS at scan rate of 0.1 V s⁻¹. No redox peaks were observed from CV of the GOx-GCE, which revealed that direct electrochemistry of GOx was not achieved at conventional solid GCE. The CVs of both GOx-fMWCNT/GCE and GOx-Met/fMWCNT/GCE showed a pair of redox peaks, and the formal redox potentials (half of sum of anodic and cathodic peak potential, $E^{0'}$) are -0.4 V and -0.39 V (vs. SCE), respectively. The CVs of GOx-Pd@Met/fMWCNT/GCE shows a pair of well-defined and nearly symmetric redox couple at $E^{0'}$ of -0.38 V with very low ΔE_p of 30 mV. Obviously, this redox couple can be assigned to the oxidation and reduction of the FAD center of GOx at the

GOx-Pd@Met/fMWCNT modified GCE.³⁴ Furthermore, the ratio of the anodic peak current (I_{pa}) and cathodic peak current (I_{pc}) is approximate to 1 revealing a fast electron transfer process between the redox center of GOx and the electrode surface.³⁵ In addition, both I_{pc} and I_{pa} of GOx-Pd@Met/fMWCNT modified GCE were 4 and 2.1 fold higher than that of GOx-fMWCNT/GCE and GOx-Met/fMWCNT/GCE, respectively. The enhanced redox peak currents and very low ΔE_p value indicate that GOx is highly immobilized onto the surface of electrode owing to its strong interaction with Pd@Met/fMWCNT nanocomposite. The plausible reason for this fascinating behavior is the large surface area, effective interaction and high conductivity of Pd@Met/fMWCNT nanocomposite offered by the synergistic effect and operative connection of two highly conducting materials PdNPs and fMWCNT.

According to Laviron's equation,³⁶ integrating both the cathodic and anodic peaks of the CVs, the surface coverage of GOx on the electrode surface of GOx-Pd@Met/fMWCNT/GCE was estimated to be 4.17×10^{-10} mol cm⁻². This value is much larger than the theoretical value (2.86×10^{-12} mol cm⁻²) for the monolayer of GOx on the bare electrode surface,³⁵ suggesting that immobilized GOx take part in the direct electron transfer.

The redox currents of the GOx-Pd@Met/fMWCNT/GCE were dependent on the scan rates. Fig. 6 showed the cyclic voltammograms of the GOx-Pd@Met/fMWCNT/GCE in 0.1 M PBS (pH 7.0) at various scan rates. It could be seen that the redox peak currents increase and the redox peak potentials shift simultaneously with the increase of scan rates, and the peak-to-peak separation become greater, indicating the more irreversible of the electrode process. The redox peak currents had almost the same values in the selected range of scan rates, which indicated that all the electroactive FAD center in GOx(FAD) was reduced to GOx(FADH₂) on the forward scan and the GOx(FADH₂) was reoxidized to GOx(FAD) on the reverse scan. The redox peak currents increased linearly with the scan rate from 0.01 to 0.3 Vs⁻¹, as shown in the insert of Fig. 6. The relationships of the redox peak currents (I_p)

with scan rate (v) were further investigated with two well-defined straight lines got as I_{pa} (μA) = $1.36+13.626v$ (Vs^{-1}) ($R^2=0.9981$) and I_{pc} (μA)= $-1.62-16.682v$ (Vs^{-1}) ($R^2=0.9981$), respectively. The experimental results prove that this redox process is a typical surface-controlled electrode process.³⁷

"Figure 6"

The charge-transfer rate constant (k_s) of the immobilized GOx on the Pd@Met/fMWCNT/GCE can be estimated based on Laviron equation:³⁸

$$\log k_s = \alpha \log(1-\alpha) + (1-\alpha)\log \alpha - \log(RT/nFv) - (1-\alpha) \alpha F \Delta E_p / 2.3RT \quad (1)$$

Taking an electron transfer coefficient α of 0.5, and a scan rate 0.3 mVs^{-1} , $\Delta E_p = 0.13 \text{ V}$, the rate constant calculated to be 3.24 s^{-1} , which is larger than those of at GOx/fMWCNT/GCE (1.74 s^{-1}). This result implied that Pd@Met/fMWCNT has more effective sites on the surface for interaction with the reactive center of GOx, leading to improve the communication between active site of GOx and electrode. Also, the k_s value of GOx at GOx-Pd@Met/fMWCNT/GCE is higher than that of GOx immobilized on a functionalized carbon nanotubes within a dihexadecylphosphate film (1.69 s^{-1})³⁹ and GOx incorporated in biomediated gold nanoparticles-carbon nanotubes composite film (2.2 s^{-1}),⁴⁰ GOx immobilized onto graphene nanosheets and carbon nanospheres mixture (2.64 s^{-1})⁴¹ and GOx immobilized on graphene quantum dots modified carbon ceramic electrode (1.12 s^{-1}),⁴² suggesting that the immobilized GOx on the Pd@Met/fMWCNT nanocomposite achieved a relative fast electron transfer process. This can be as a result of the synergistic effect of PdNPs and fMWCNT is of vital importance to the electron transfer between the GOx and the electrode.

3.4 Performance of the proposed glucose biosensor

Fig. 7A shows CVs of GOx-Pd@Met/fMWCNT/GCE in (pH 7.0) N₂-saturated PBS (curve a), air-saturated PBS (curve b) and O₂-saturated PBS (curve c) at scan rate 0.1 Vs⁻¹. A clear increase in cathodic peak current and a simultaneous decrease in anodic peak current of GOx in the air-saturated PBS (curve b) and O₂-saturated PBS (curve c) can be observed, demonstrating an obvious electrocatalytic process toward the reduction of dissolved oxygen according to following equations:⁴³



Fig. 7B shows the CVs of GOx-Pd@Met/fMWCNT/GCE in the air-saturated stirring PBS (pH 7.0) containing different concentrations of glucose. As it can be seen, with the increasing of glucose concentration the reduction current response decreased. On the other words, as shown in the Eq. 4, the enzyme-catalyzed reaction decreases GOD(FAD) and curbs the electrochemical reaction:²⁹



"Figure 7"

Fig. 8A shows the amperometric response of the GOx-Pd@Met/fMWCNT/GCE upon successive additions of glucose to 0.1 M PBS (pH 7.0) at a detection potential of -0.47 V. Immediately after the addition of glucose, the response increases and reaches 95% of the steady state value within ~3 s, suggesting that the GOx-Pd@Met/fMWCNT/GCE responds rapidly to the change of the substrate concentration. The electrode linearly responds to glucose at lower concentrations and attains saturation levels at higher concentrations (Fig. 8B). The response displays a good linear range from 4 to 1500 μM with a correlation coefficient of 0.9987 and a slope of 0.0343 ± 0.2 μA μM⁻¹. The limit of detection (S/N=3) is

estimated to be ca. $1.4 \pm 0.04 \mu\text{M}$, which is comparable with or, in most cases, broader than the reported value of $1.0 \mu\text{M}$ glucose oxidase in electropolymerized poly(o-phenylenediamine) film on Pt nanoparticles-polyvinylferrocenium,²⁵ 0.01 mM glucose biosensor based on glucose oxidase immobilized on AuPt nanoparticle-carbon nanotube-ionic liquid hybrid coated electrode,⁴⁴ 0.2 mM glucose oxidase incorporated in biomediated gold nanoparticles-carbon nanotubes composite film,⁴⁰ $100 \mu\text{M}$ graphene/polyaniline/Au nanoparticles/glucose oxidase biocomposite modified electrode,⁴⁵ 0.16 mM glucose oxidase immobilized on reduced graphene oxide and silver nanoparticles nanocomposite³⁰ and $1.7 \mu\text{M}$ glucose oxidase on three-dimensional interpenetrating, porous graphene modified electrode.³⁵ These results indicate that the biosensor possesses high bioelectrocatalytic activity toward glucose detection. When the glucose concentration is higher than 1.5 mM , a response plateau is observed, which indicate the characteristics of the Michaelis-Menten kinetic mechanism. Based on the Lineweaver-Burk equation, the apparent Michaelis-Menten constant ($K_{\text{app}}^{\text{M}}$) can be obtained (Eq. (5)).⁴⁶

$$(1/I_{\text{ss}}) = (1/I_{\text{max}}) + (K_{\text{app}}^{\text{M}}/I_{\text{max}}C)$$

where I_{ss} is the steady-state current after the addition of the substrate, C is the bulk concentration of the substrate, and I_{max} is the maximum current measured under saturation conditions. From the Lineweaver-Burk plot (Fig. 8C), the $K_{\text{app}}^{\text{M}}$ value is calculated to be 0.48 mM , which is significantly smaller than 2.95 mM of GOx immobilized onto glassy carbon electrode modified with nitrophenyl diazonium salt⁴⁷ and also smaller than 0.6 mM GOx immobilized onto graphene/polyaniline/gold nanoparticles nanocomposite,²⁷ and 0.71 mM for GOx immobilized onto graphene quantum dots.⁴² This result revealed that the Pd@Met/fMWCNT nanocomposite provides an operative microenvironment for GOx to

retain its native biological activity due to the effective adsorption of GOx and the electrical network formed through direct binding of PdNPs with the fMWNTs.

"Figure 8"

3.5 Stability and reproducibility of the biosensor

The GOx–Pd@Met/fMWCNT/GCE was stored at 4 °C, and the stability was investigated by measuring the cyclic voltammogram periodically. The results indicated that the peak potentials and currents of biosensor were stable for ten days and then decreased gradually. Also, the cyclic voltammetric peak potentials appeared at the same position with the peak current decreasing by 16% compared with the initial response after 1 month. The reproducibility of the proposed biosensor towards glucose detection was also studied. The R.S.D. of inter-electrode responses to 100 µM glucose at five different electrodes was 4.54% while the R.S.D. of intra-electrode responses to five-times repeated additions of 100 µM glucose was 3.1%. These results indicate that the GOx–Pd@Met/fMWCNT/GCE was very efficient for retaining high enzymatic activity and preventing enzyme leakage from the Pd@Met/fMWCNT nanocomposite, which was very important for the development of the proposed biosensor in low-cost application.

3.6 Selectivity and real sample analysis

Some potential substrates in biological system may influence the detection of glucose in practical use of the biosensor, so the selectivity of biosensor was evaluated by glucose measurements in the presence of a number of interfering substances such as ascorbic acid (AA), uric acid (UA), dopamine (DA) and acetaminophen (AC). The current response obtained in the mixture of glucose and the mentioned interfering species was compared with the results obtained in the pure glucose solution. As shown in Table 1, all these interferences

have little influence on the glucose determination. Similarly, the interfering signals from 0.5 mM l-cysteine, and 1.0 mM Ca^{2+} , Mg^{2+} and 2.0 mM Cl^- do not influence the performance of the biosensor. This result indicates that the proposed biosensor has high selectivity for glucose and is suitable for practical applications. The performance of the biosensor for practical application in the analysis of real samples was investigated using human serum and urine samples under optimum conditions without any sample pretreatment except a dilution step with PBS (pH 7.0) by the standard additional method. The determined results were compared with those obtained by a spectrophotometric method on a standard clinical laboratory. The results are summarized in Table 2. As shown, the results obtained by the biosensor are in good agreement with those measured by the spectrophotometric method in the clinical laboratory and the recovery is satisfied.

"Table 1"

"Table 2"

4. Conclusions

We have reported here a successful way to deposit PdNPs on functionalized MWCNT surface using metformine with high dispersion and effective adhesion without affecting the electronic network of the tubes. Pd@Met/fMWCNT nanocomposite has been successively applied for the adsorption of GOx to achieve the DET of GOx and fabricating electrochemical glucose biosensor. The favorable results mainly attribute to the synergistic effects of PdNPs with Met/fMWCNT in immobilization of GOx and the electrical conductivity of the nanocomposite film. Furthermore, the modified electrode possesses good selectivity, stability and reproducibility. Therefore, proposed biosensor offers an effective method for the determination of glucose in real samples and has potential applications in the

study of the direct electrochemistry of redox proteins/enzymes and the development third-generation biosensors.

Acknowledgement

We would like to thank the Hakim Sabzevari University for its financial support.

References

- 1 V. K. Gupta, M. R. Ganjali, P. Norouzi, H. Khani, A. Nayak, and Shilpi Agarwal, *Crit. Rev. Anal. Chem.* 2011, **41**, 282-313
- 2 R. Jain, V. K. Gupta, N. Jadon, and K. Radhapyari, *Anal. Biochem.* 2010, **407**, 79–88.
- 3 V. K. Gupta, A. K. Singh, S. Mehtab, and B. Gupta, *Anal. Chim. Acta* 2006, **566**, 5-10.
- 4 V. K. Gupta, A. K. Singh, M. Al Khayat, and B. Gupta, *Anal. Chim. Acta* 2007, **590**, 81-90.
- 5 V. K. Gupta, R. Prasad, P. Kumar, and R. Mangla, *Anal. Chim. Acta* 2000, **420**, 19-27.
- 6 R. N. Goyal, V. K. Gupta, and S. Chatterjee, *Electrochim. Acta* 2008, **53**, 5354-5360.
- 7 S. K. Arya, T. S. Pui, C. C. Wong, S. Kumar and A. R. A. Rahman, *Langmuir* 2013, **29**, 6770-6777.
- 8 V. K. Gupta, A. K. Jain, and G. Maheshwari, *Talanta* 2007, **72**, 1469-1473.
- 9 V. K. Gupta, A.K. Jain, S. Agarwal, and G. Maheshwari, *Talanta* 2007, **71**, 1964-1968.
- 10 S. Alwarappan, G. Liu, and C.-Z. Li, *Nanomedicine* 2010, **6**, 52-57.
- 11 L. Qu and L. Dai, *J. Am. Chem. Soc.* 2005, **127**, 10806-10807.
- 12 S. Alwarappan, S. Prabhulkar, A. Durygin, and C.-Z. Li, *J. Nanosci. Nanotechnol.* 2009, **9**, 2991-2996.
- 13 R. N. Goyal, V. K. Gupta, and S. Chatterjee, *Sens. Actuators B: Chem.* 2010, **149**, 252-258.
- 14 R. N. Goyal, V. K. Gupta, and S. Chatterjee, *Talanta* 2008, **76**, 662-668.
- 15 S. Dhibar and C. K. Das, *Ind. Eng. Chem. Res.* 2014, **53**, 3495-3508.
- 16 M. Baghayeri, E. N. Zare and M. Namadchian, *Sens. Actuators B: Chem.* 2013, **188**, 227-234.
- 17 A. Senthil Kumar, P. Gayathri, P. Barathi and R. Vijayaraghavan, *J. Phys. Chem. C* 2012, **116**, 23692-23703.
- 18 P. C. Ma, B. Z. Tang and J. -K. Kim, *Carbon* 2008, **46**, 1497-1505.

- 19 S. Zheng, J. Hu, L. Zhong, L. Wan and W. Song, *J. Phys. Chem. C* 2007, **111**, 11174-11179.
- 20 H. Ahmar, S. Keshipour, H. Hosseini, A. R. Fakhari, A. Shaabani and A. Bagheri, *J. Electroanal. Chem.* 2013, **690**, 96-103.
- 21 V. Georgakilas, D. Gournis, V. Tzitzios, L. Pasquato, D. M. Guldi and M. Prato, *J. Mater. Chem.* 2007, **17**, 2679-2694.
- 22 Z. -P. Sun, X. -G. Zhang, Y. -Y. Liang and H. -L. Li, *Electrochem. Commun.* 2009, **11**, 557-561.
- 23 R. Yu, L. Chen, Q. Liu, J. Lin, K. Tan, S. C. Ng, H. S. O. Chan, G. -Q. Xu and T. S. Andy Hor, *Chem. Mater.* 1998, **4756**, 718-722.
- 24 R. Zanella, E. V. Basiuk, P. Santiago, V. A. Basiuk, E. Mireles, I. Puente-Lee and J. M. Saniger, *J. Phys. Chem. B* 2005, **109**, 16290-16295.
- 25 E. Turkmen, S. Z. Bas, H. Gulce and S. Yildiz, *Electrochim. Acta* 2014, **123**, 93-102.
- 26 X. Zeng, X. Li, L. Xing, X. Liu, S. Luo, W. Wei, B. Kong and Y. Li, *Biosens. Bioelectron.* 2009, **24**, 2898-2903.
- 27 Q. Xu, S. Gu, L. Jin, Y. Zhou and Z. Yang, *Sens. Actuators B: Chem.* 2014, **190**, 562-569.
- 28 M. A. Kamyabi, N. Hajari, A. P. F. Turner and A. Tiwari, *Talanta* 2013, **116**, 801-808.
- 29 T. Homma, D. Sumita, M. Kondo, T. Kuwahara and M. Shimomura, *J. Electroanal. Chem.* 2014, **712**, 119-123.
- 30 S. Palanisamy, C. Karupiah and S. -M. Chen, *Colloids Surf., B* 2014, **114**, 164-169.
- 31 Y. Yu, Z. Chen, S. He, B. Zhang, X. Li and M. Yao, *Biosens. Bioelectron.* 2014, **52**, 147-152.
- 32 C. W. Hills, N. H. Mack and R. G. Nuzzo, *J. Phys. Chem. B* 2003, **107**, 2626-2636.
- 33 Z. Yang, X. Huang, R. Zhang, J. Li, Q. Xu and X. Hu, *Electrochim. Acta* 2012, **70**, 325-330.

- 34 V. Mani, B. Devadas and S. -M. Chen, *Biosens. Bioelectron.* 2013, **41**, 309-315.
- 35 M. Cui, B. Xu, C. Hu, H. B. Shao and L. Qu, *Electrochim. Acta* 2013, **98**, 48-53.
- 36 J. -Y. Sun, K. -J. Huang, S. -F. Zhao, Y. Fan and Z. -W. Wu, *Bioelectrochemistry* 2011, **82**, 125-130.
- 37 K. -J. Huang, J. -Y. Sun, D. -J. Niu, W. -Z. Xie and W. Wang, *Colloids Surf., B* 2010, **78**, 69-74.
- 38 E. Laviron, *J. Electroanal. Chem.* 1979, **101**, 19-28.
- 39 B. C. Janegitz, R. Pauliukaite, M. E. Ghica, C. M. A. Brett and O. Fatibello-Filho, *Sens. Actuators B: Chem.* 2011, **158**, 411-417.
- 40 H. Zhang, Z. Meng, Q. Wang and J. Zheng, *Sens. Actuators B: Chem.* 2011, **158**, 23-27.
- 41 H. Yin, Y. Zhou, X. Meng, K. Shang and S. Ai, *Biosens. Bioelectron.* 2011, **30**, 112-117.
- 42 H. Razmi and R. Mohammad-rezaei, *Biosens. Bioelectron.* 2013, **41**, 498-504.
- 43 R. Cui, Z. Han, J. Pan, E. S. Abdel-Halim and J. -J. Zhu, *Electrochim. Acta* 2011, **58**, 179-183.
- 44 Y. Zhang, G. Guo, F. Zhao, Z. Mo, F. Xiao, and B. Zeng, *Electroanalysis* 2010, **22**, 223-228.
- 45 F. -Y. Kong, S. -X. Gu, W. -W. Li, T. -T. Chen, Q. Xu and W. Wang, *Biosens. Bioelectron.* 2014, **56**, 77-82.
- 46 M. Baghayeri, E. N. Zare and M. M. Lakouraj, *Biosens. Bioelectron.* 2014, **55**, 259-265.
- 47 Z. Nasri and E. Shams, *Electrochim. Acta* 2013, **112**, 640-647.

Figure and scheme captions

Scheme 1. (A) Synthetic pathway of Pd@Met/fMWCNT nanocomposite. (B) The electrode construction pathway.

Fig. 1. TEM images of (a) Met/fMWCNT and (b) Pd@Met/fMWCNT nanocomposite.

Fig. 2. XRD patterns of Pd@Met/fMWCNT nanocomposite.

Fig. 3. FT-IR spectra of (a) MWCNT, (b) MWCNT-COOH, (c) MWCNT-COCl, (d) Met/fMWCNT, and (e) Pd@Met/fMWCNT.

Fig. 4. FT-IR spectra of (a) native GOx, (b) pure Pd@Met/fMWCNT nanocomposite and (c) GOx-Pd@Met/fMWCNT.

Fig. 5. (A) Nyquist plots of (a) bare GCE, (b) Pd@Met/fMWCNT/GCE, and (c) GOx-Pd@Met/fMWCNT/GCE in 1.0 mM $K_3Fe(CN)_6/K_4Fe(CN)_6$ with 0.10 M KCl as the supporting electrolyte. AC amplitude: 5 mV; frequency range: 0.1– 10^5 Hz. (B) CVs of the (a) GOx-GCE, (b) GOx-fMWCNT/GCE, (c) GOx-Met/fMWCNT/GCE, and (d) GOx-Pd@Met/fMWCNT/GCE in N_2 -saturated 0.1 M pH 7.0 PBS at scan rate of $0.1 V s^{-1}$.

Fig. 6. CVs of GOx-Pd@Met/fMWCNT/GCE in 0.1 M PBS (pH 7.0) at different scan rates of (a) 0.01, (b) 0.02, (c) 0.04, (d) 0.06, (e) 0.08, (f) 0.10, (g) 0.14, (h) 0.18, (i) 0.22, (j) 0.26 and (k) $0.30 V s^{-1}$. Inset: plot of the peak current against the scan rate.

Fig. 7. (A) CVs of GOx-Pd@Met/fMWCNT/GCE in N_2 -saturated (a), air-saturated (b) and O_2 -saturated (c) 0.1 M pH 7.0 PBS at $0.06 V s^{-1}$, respectively. (B) CVs of GOx-Pd@Met/fMWCNT/GCE in air-saturated 0.1 M pH 7.0 PBS containing 0, 0.2, 0.4 and 0.6 mM glucose (from (d) to (g)) at scan rate of $0.1 V s^{-1}$.

Fig. 8. Amperometric response of the glucose biosensor to successive addition of different concentration of glucose into a stirring air-saturated 0.1 M PBS (pH 7.0) at the working potential of -0.47 V. Inset a: plot of electrocatalytic peak current vs. concentration of glucose. Inset b: plot of the reciprocal of steady-state current (I_{ss}) versus the reciprocal of glucose concentration for the GOx-Pd@Met/fMWCNT/GCE.

Table 1

Effects of possible interfering agents on the determination of glucose at GOx–Pd@Met/fMWCNT/GCE.

Substrates ^a	Response current ^b (μA)	Current ratio ^c
Glucose	35.5± 0.06	-
Glucose + AA	35.8± 0.05	1.00
Glucose + UA	36.0± 0.03	1.01
Glucose + DA	35.4± 0.06	99.7
Glucose + AC	35.4± 0.04	99.7

^aThe concentrations of substrates were glucose: 1.0 mM; AA: 2.0 mM; UA: 3.0 mM, DA: 2.0 mM and AC 1.0 mM.

^bAverage of five determinations ± standard deviation.

^cCurrent ratio is the current from a mixture of interfering substances and glucose (with mentioned concentrations) vs. the current from 1.0 mM glucose alone. Assay solution: 0.1 M pH 7.0 PBS.

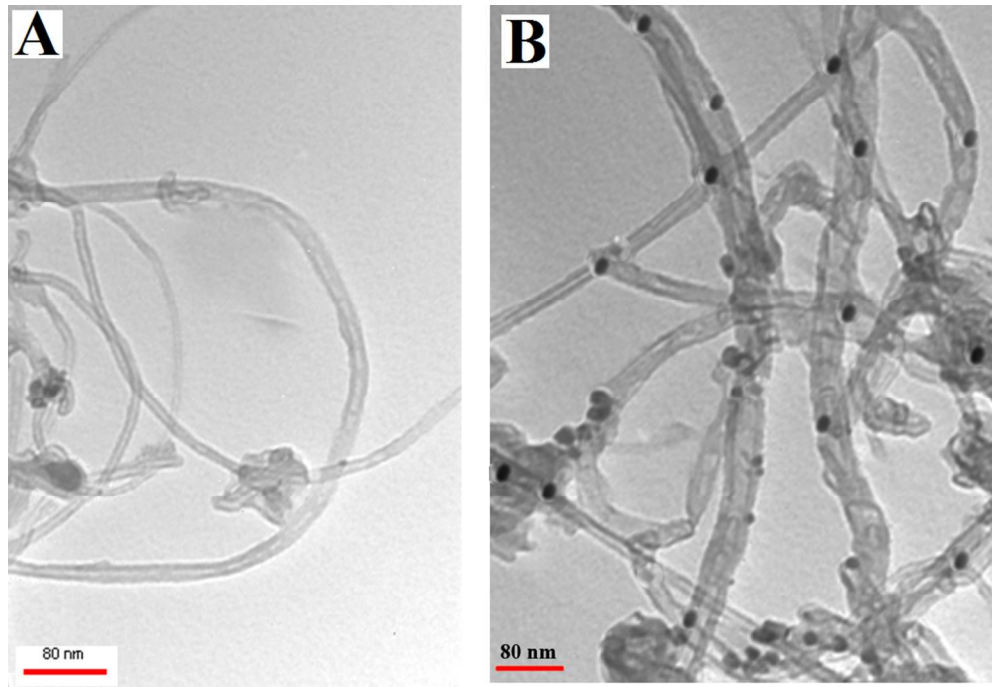
Table 2

Results of the glucose determination and the recovery test for real samples (n=5).

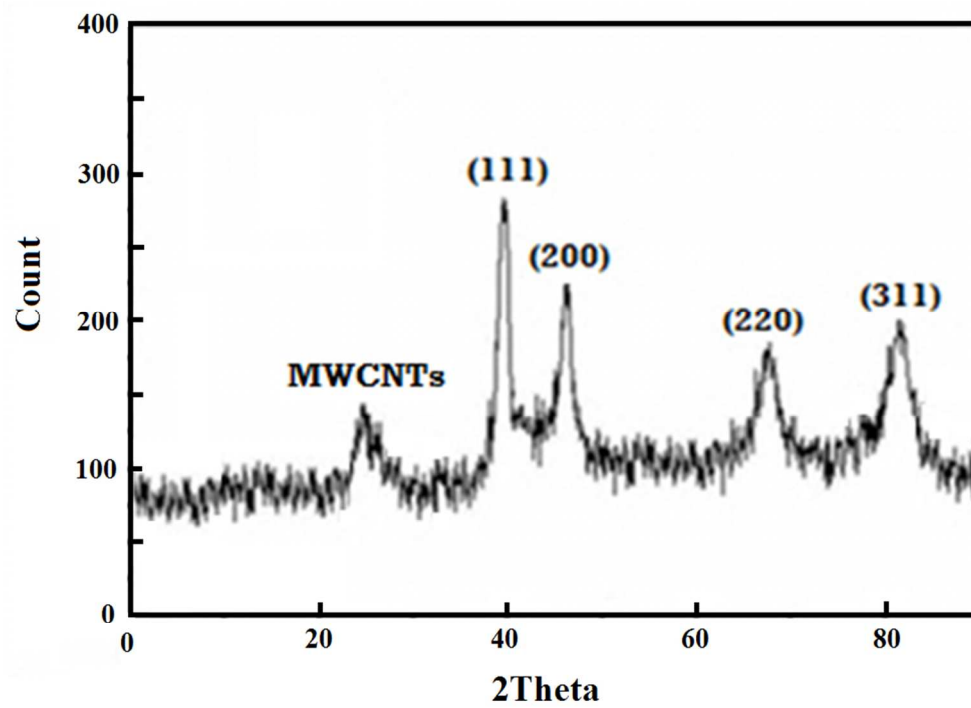
Serum sample	Added (mM)	Found (mM)	Determined by spectrophotometry	Recovery (%)
A	0	0.64±0.07	0.67	-
	0.3	0.96±0.06		102.1
	0.5	1.13±0.03		99.12
B	0	0.78±0.05	0.76	-
	0.2	0.97±0.05		98.97
	0.6	1.40±0.04		101.4
C	0	-	-	-
	0.2	0.193±0.05	0.21	96.5
	0.4	0.41±0.04	0.41	102.5
D	0	-	-	-
	0.3	0.306±0.04	0.295	102
	0.5	0.507±0.07	0.51	101.4

A and B samples of glucose in human serum.

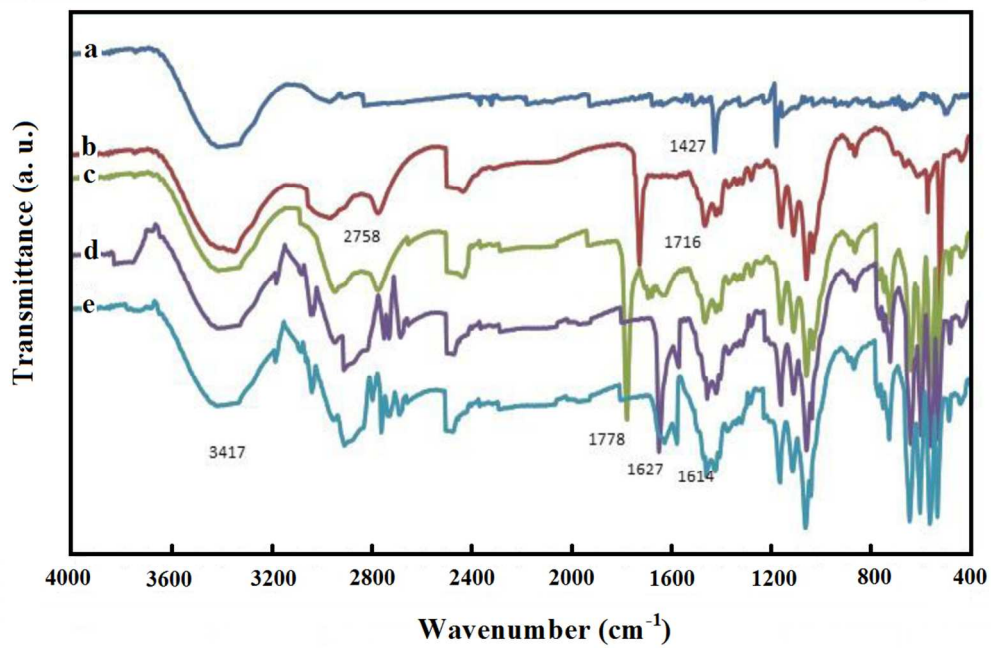
C and D samples of glucose in human urine.



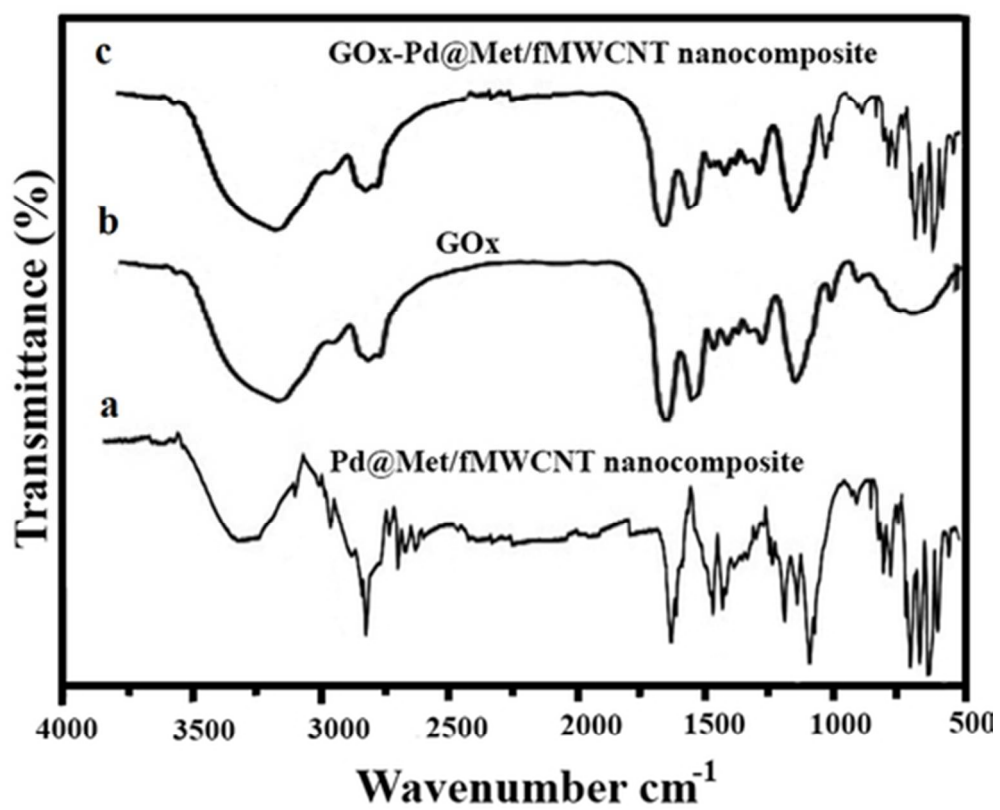
241x165mm (119 x 119 DPI)



211x153mm (120 x 120 DPI)



257x170mm (120 x 120 DPI)



42x35mm (300 x 300 DPI)

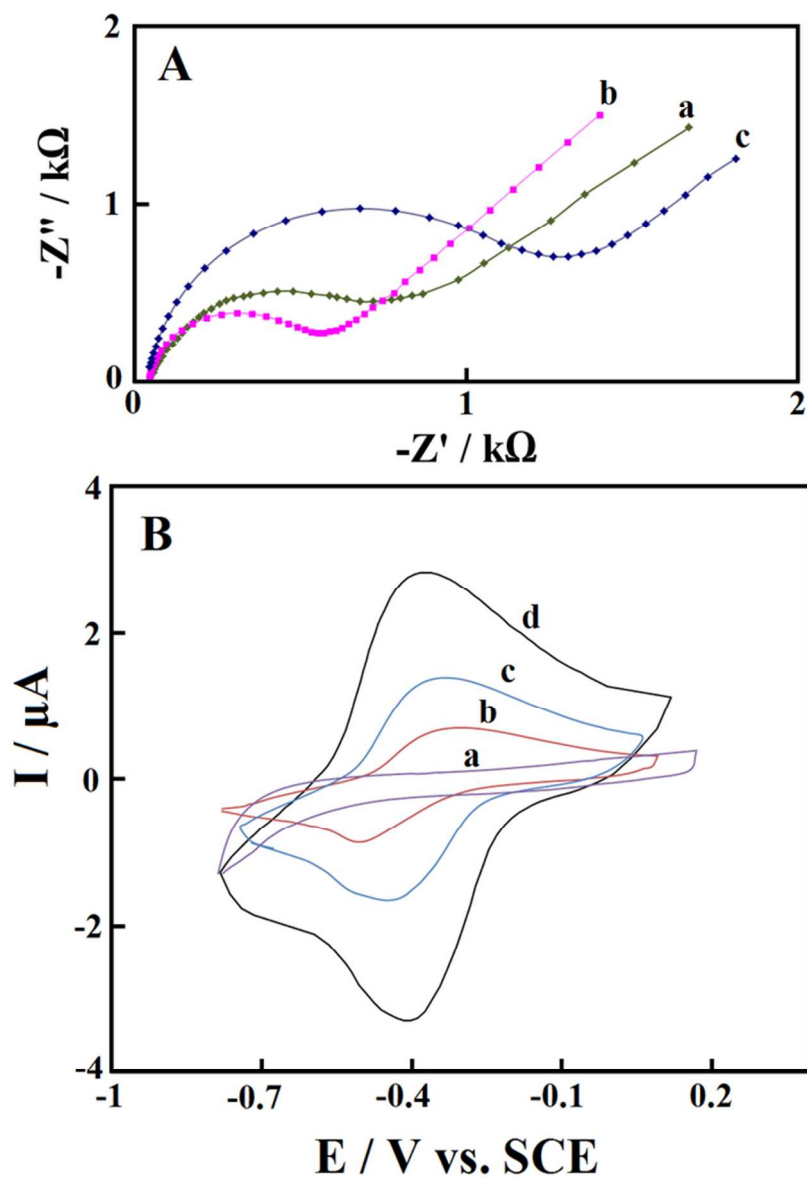
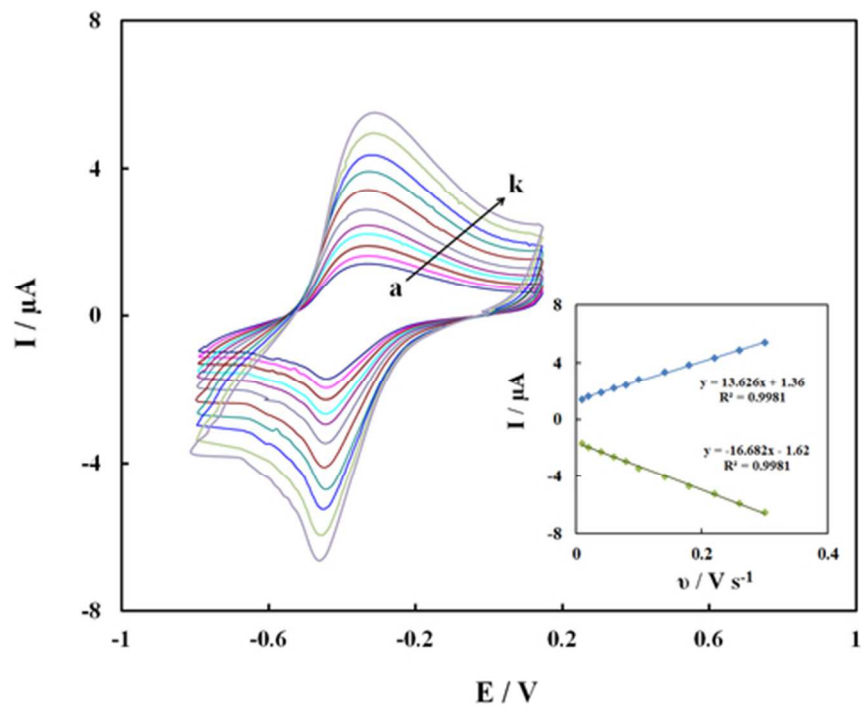
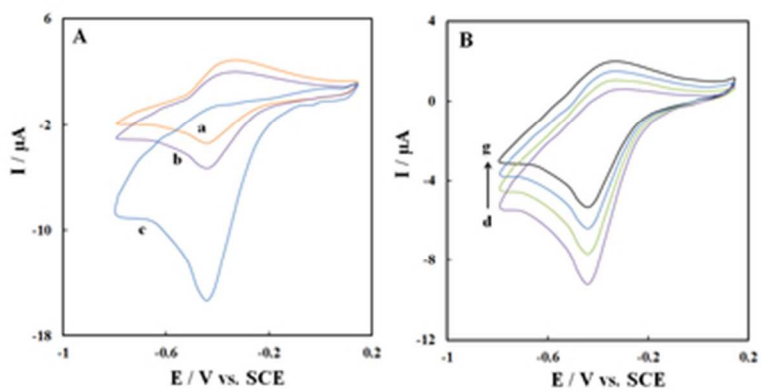


Fig. 5. (A) Nyquist plots of (a) bare GCE, (b) Pd@Met/fMWCNT/GCE, and (c) GOx-Pd@Met/fMWCNT/GCE in 1.0 mM $K_3Fe(CN)_6/K_4Fe(CN)_6$ with 0.10 M KCl as the supporting electrolyte. AC amplitude: 5 mV; frequency range: 0.1–105 Hz. (B) CVs of the (a) GOx-GCE, (b) GOx-fMWCNT/GCE, (c) GOx-Met/fMWCNT/GCE, and (d) GOx-Pd@Met/fMWCNT/GCE in N_2 -saturated 0.1 M pH 7.0 PBS at scan rate of 0.1 $V s^{-1}$.

61x88mm (300 x 300 DPI)



50x38mm (300 x 300 DPI)



32x17mm (300 x 300 DPI)

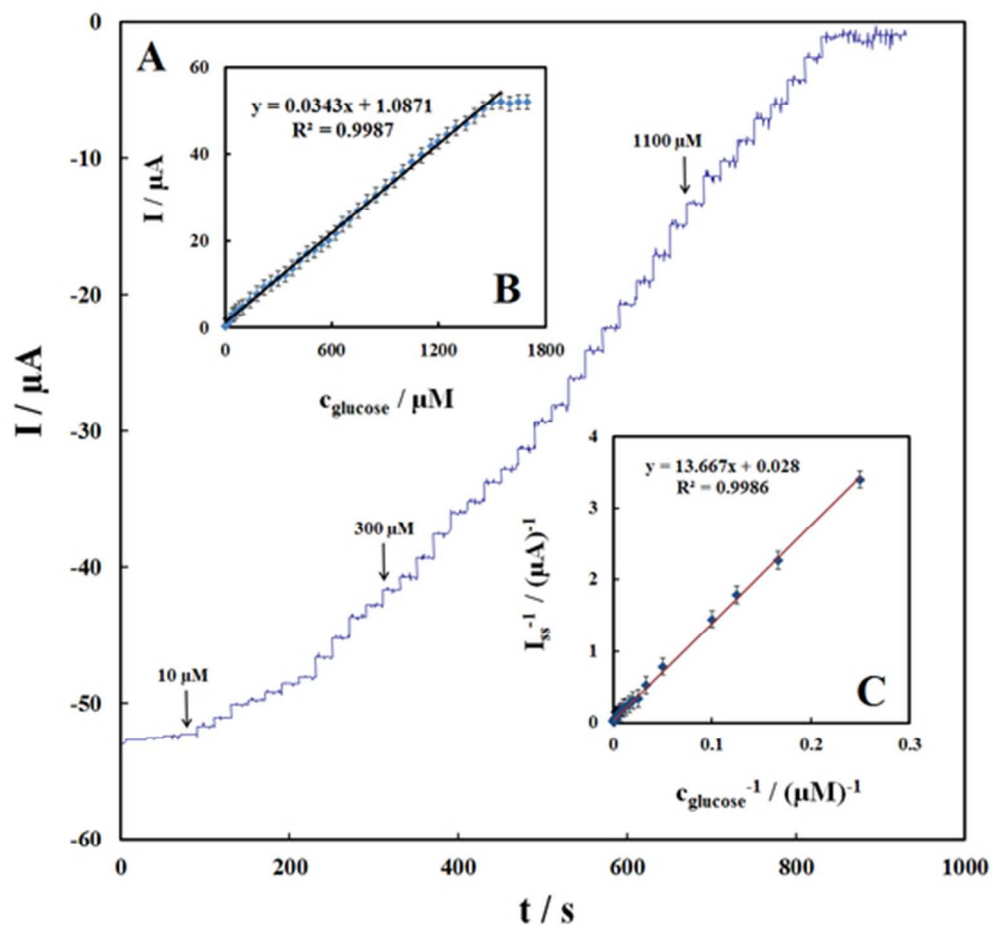


Fig. 8. Amperometric response of the glucose biosensor to successive addition of different concentration of glucose into a stirring air-saturated 0.1 M PBS (pH 7.0) at the working potential of -0.47 V. Inset a: plot of electrocatalytic peak current vs. concentration of glucose. Inset b: plot of the reciprocal of steady-state current (I_{ss}) versus the reciprocal of glucose concentration for the GOx-Pd@Met/fMWCNT/GCE. 45x43mm (300 x 300 DPI)

